JOURNAL OF SOLID STATE CHEMISTRY 53, 174–183 (1984)

Next-Nearest Neighbor Effects in the Mössbauer Spectra of (Cr,Al) Spinels

M. D. OSBORNE,* M. E. FLEET, AND G. M. BANCROFT

Departments of Geology and Chemistry, University of Western Ontario, London, Ontario N6A 5B7, Canada

Received October 4, 1983; in revised form January 20, 1984

Fe^{2+} T-site quadrupole splitting observed in the Mössbauer spectra of synthetic chromite-hercynite spinels ($Fe(Cr_{1-x}Al_x)_2O_4$, with $x = 0$ to 1.5) is systematically related to the substitution of octahedrally coordinated cations in the next-nearest neighbor coordination sphere. Conditions of synthesis include dry reagents contained in a stainless-steel crucible and enclosed in an evacuated silica-glass tube, held at 1250°C for up to 4 days. A simple singlet spectrum for $FeCr_2O_4$ changes with progressive Al substitution into a broadened doublet spectrum, with quadrupole splitting of 1.28 mm/sec and line half-width of 0.82 mm/sec, for $FeCrAlO_4$. Partial quadrupole splitting theory is used to calculate the quadrupole splittings for individual next-nearest neighbor configurations. Bulk quadrupole splitting is calculated relative to the statistical distribution of possible next-nearest neighbor configurations. Calculated quadrupole splittings are in good agreement with those obtained for unconstrained two-peak fits, at room temperature and at low and high temperature. Also, predicted spectral details are resolved in low temperature spectra. The local site distortion responsible for the quadrupole splitting appears to be associated with spatial accommodation of substituent Al^{3+} cations.

Introduction

Normal spinels such as $Fe(Cr,Al)_2O_4$ have divalent cations positioned on the tetrahedral (T) site and trivalent cations positioned on the octahedral (M) site. Although the tetrahedral site has perfect T_d symmetry in the ideal structure, cation substitutions in the solid solution series, and apparently even crystalline defects in $FeAl_2O_4$ (Refs. (*1, 2*) and work in progress), result in a lower symmetry for the crystalline field about individual T^{2+} cations. Local distortion about the T-site Fe^{2+} cations in normal spinel compositions is confirmed by many diverse optical and Mössbauer investigations (*3, 4*). In the spinel structure, the T-site has a second coordination sphere of four threefold clusters of octahedrally coordinated, trivalent cations. Since the cubic spinel structure of $Fe(Cr,Al)_2O_4$ has a very wide field of stability (the Verwey phase transition occurs at 10 K in $FeCr_2O_4$ (*5*) and has not been observed at low temperatures in $FeAl_2O_4$) and charge transfer or partial inversion effects are not evident in the Mössbauer spectra, the $Fe(Cr,Al)_2O_4$ system is ideally suited to the study of the effects of next-nearest neighbor cation substitutions on the electric field gradient (EFG) of tetrahedrally coordinated Fe^{2+}.

* Present address: Department of Chemistry, Arizona State University, Tempe, Arizona 85287.

0022-4596/84 $3.00

This paper investigates the quadrupole splitting (QS) within the $Fe(Cr,Al)_2O_4$ solid solution using Mössbauer spectroscopy in the temperature range 110–500 K, and quantitatively accounts for its variation with partial quadrupole splitting theory (pqs). A preliminary report is given in Bancroft *et al.* (*6*).

Previous workers have reported the Mössbauer spectrum of synthetic $FeCr_2O_4$ and $FeCr_2S_4$ as a singlet due to iron at the tetrahedral site (*7*) and next-nearest neighbor effects have long been implicated in the origin of quadrupole splitting in the solid–solutions $FeCr_2O_4$–Fe_3O_4 (*8*) and $FeCr_2S_4$–$FeRh_2S_4$ (*9*). The spinels $FeNiAlO_4$ and $FeNiCrO_4$ were studied by Mizoguchi and Tanaka (*7*) who also attributed the quadrupole split doublet they observed to the presence of divalent and trivalent cations on the octahedral site. The resulting charge anisotropies were statistically related to the various quadrupole splittings obtained experimentally.

Partial quadrupole splitting theory has been applied successfully to interpretation of quadrupole splittings in inorganic compounds with low spin Fe^{2+} and multiple ligand species (*10*). Its application to $Fe(Cr,Al)_2O_4$ spinels involves high-spin Fe^{2+} and only one ligand type. However, local ligand charge density about individual T-site Fe^{2+} cations will vary with octahedral cation substitution. Since each stereochemically distinct oxygen atom has an essentially constant charge density, we make the assumption that it is associated with a specific *partial* quadrupole splitting. Partial quadrupole splittings are additive, combining to give the individual T-site quadrupole splitting. The latter are statistically related to the observed composite quadrupole splitting. We emphasize that the partial quadrupole splitting calculation is essentially empirical and that the values derived for each stereochemically distinct oxygen (or corresponding next-nearest neighbor cation configuration) do not reflect on the origin of the characteristic charge density.

Experimental

Mirror-image Mössbauer spectra were recorded in 512 channels using an Austen Science Associates spectrometer and a 50-mCi ^{57}Co in Pd source. The spectrometer was calibrated using iron foil. Spectra, obtained on thin powdered samples, were allowed to accumulate at least 3×10^6 counts per channel so that peak height was greater than 10^5 counts. Low temperature runs were made with a copper cold finger suspended in a reservoir of liquid nitrogen resulting in a sample temperature of approximately 110 K, just above the Verwey temperature observed for pure $FeCr_2O_4$ (*5*). High temperature spectra were taken on powdered samples in a Ranger Scientific Model 700 furnace under vacuum.

The spectra were fitted to pure Lorentzian lineshapes and evaluated by comparison with natural and synthetic chromite parameters previously described in Osborne *et al.* (*11*). Component peak half-widths within a doublet were constrained to be equal but half-widths between doublets were unconstrained. The resultant large half-widths are considered indicative of a Gaussian component of the peak shape stemming from next-nearest neighbor interactions (*11*). Constraints on peak areas are detailed below.

Figure 1 shows a composite of spectra from the solid–solution $FeCr_2O_4$–$FeCrAlO_4$. Figures 2 and 3 show details of the fits for compositions $FeCr_{1.90}Al_{0.10}O_4$ and $FeCrAlO_4$. Figure 4 shows a composite of high and low temperature spectra for sample $FeCrAlO_4$. In particular, it should be noted that Fig. 1 shows a progressive increase in quadrupole splitting and peak half-width from the initial singlet obtained for $FeCr_2O_4$ to $FeCrAlO_4$. These spectra are qualitatively similar to those previously

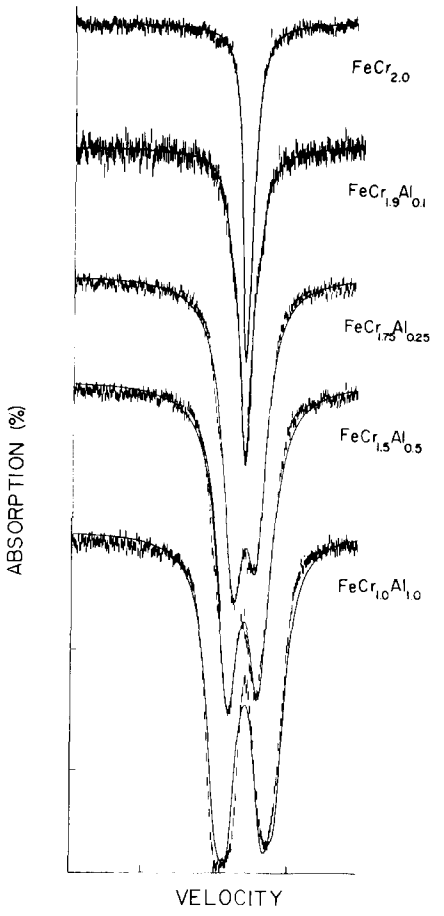

FIG. 1. Room temperature ^{57}Fe Mössbauer spectra of $FeCr_2O_4$–$FeAl_2O_4$ solid solutions (velocity in mm/sec).

published for the series $FeCr_2S_4$–$FeRh_2S_4$ (*9*). Figure 4 shows a progressive decrease in quadrupole splitting and increase in half-width as temperature increases. The low temperature spectrum of $FeCrAlO_4$ shows a clearly resolved doublet of lower quadrupole splitting and half-width nested within an outer broader doublet.

Partial Quadrupole Splitting Theory

The quadrupole splitting (*QS*) of high-spin Fe^{2+} in octahedral coordination has been related to cation site distortion by Ingalls (*12*), who found that the quadrupole

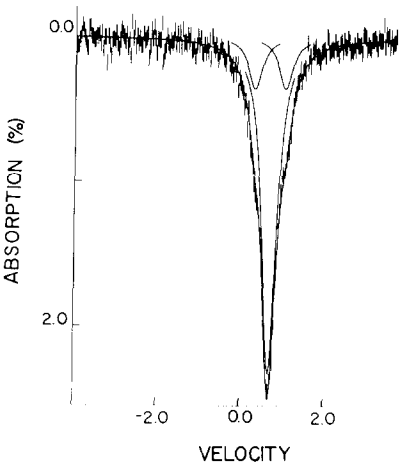

FIG. 2. Room temperature Mössbauer spectrum of $FeCr_{1.90}Al_{0.10}O_4$, showing fitted quadrupole doublet attributed to AB_3 next-nearest neighbor configuration (velocity in mm/sec).

splitting first increases rapidly, then decreases with increasing deviation from cubic symmetry. Following Gibb and Greenwood (*13*), an analogous expression to the Ingall's equation for tetrahedral coordination, giving the dependence of quadrupole splitting on cation site distortion (represented by ground state splitting) and temperature is

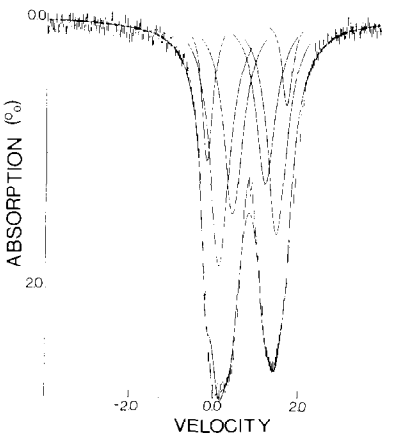

FIG. 3. Fitted room temperature Mössbauer spectrum of $FeCrAlO_4$ (velocity in mm/sec).

$$QS(T) = QS(0)[1 - e^{(-\Delta/kT)}]/[1 + e^{(-\Delta/kT)}] \quad (1)$$

where $QS(0)$ is the quadrupole splitting at 0 K, T is the temperature in degrees K, and Δ is the ground state splitting of Fe^{2+} (in cm^{-1}). A value of 4.00 mm/sec is used for $QS(0)$ (*13*) (Fig. 5). Following Ingalls (*12*), the quadrupole splitting has q_{val} and q_{lat} components. Since the local distortions of the crystalline field about T-site Fe^{2+} cations in $Fe(Cr,Al)_2O_4$ spinels are thought to be very small, q_{lat} is small compared to q_{val}. Thus the ground state splittings associated with the local site distortions must correspond to the range of Δ of Eq. (1) in which quadrupole splitting is most sensitive to distortion and almost linear with Δ (Fig. 5).

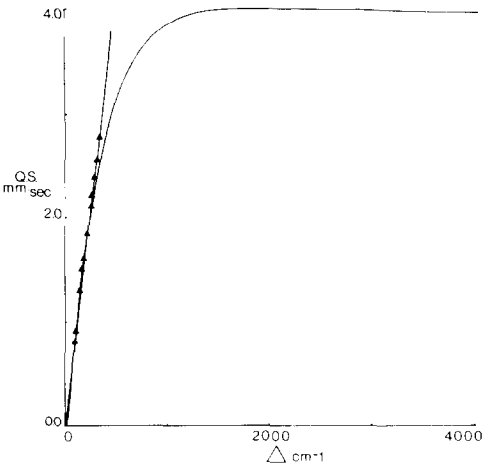

FIG. 5. Quadrupole splitting (QS) vs ground state splitting (Δ) for T site Fe^{2+} at room temperature, computed from Eq. (1).

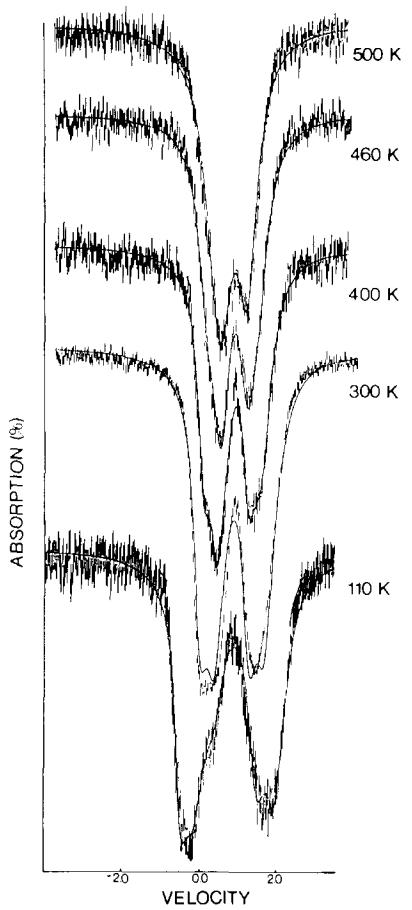

FIG. 4. High and low temperature Mössbauer spectra of $FeCrAlO_4$ (velocity in mm/sec).

As we have suggested above, the electric field gradient (EFG) on the Fe^{2+} nucleus can be varied, in principle, by atomic substitution in the second coordination sphere (the sphere of next-nearest neighbor cations). If the contribution from a specific octahedral site substitution is assumed to be constant and linear, the partial quadrupole splittings (pqs) from each cation–ligand arrangement are additive, combining to give the observed quadrupole splitting of individual T-site Fe^{2+} cations.

Each of the four oxygens surrounding a T-site Fe^{2+} cation is, in turn, bonded to three octahedral cations. The possible distributions of Cr and Al per oxygen are 3Cr, 2Cr1Al, 1Cr2Al, 3Al, which we will refer to as A, B, C, and D, respectively. According to a point charge model in which only the effective charge on the oxygens is considered, a distribution of four A, B, C, or D clusters about a Fe^{2+} cation would result in zero quadrupole splitting. However, all other possible combinations should result in an observable quadrupole splitting. These can

TABLE I

PARTIAL QUADRUPOLE SPLITTING EQUATIONS (*14*)

Components of EFG tensor	$FeABC_2$	FeA_2C_2	$FeAC_3$
V_{xx}	$-[A] + \frac{2}{3}[B] - \frac{2}{3}[C]$	$\frac{2}{3}[A] - \frac{2}{3}[C]$	$-[A] + [C]$
V_{yy}	$-[A] - [B] + 2[C]$	$-2[A] + 2[C]$	$-[A] + [C]$
V_{zz}	$2[A] - \frac{2}{3}([B] + 2[C])$	$\frac{1}{3}([A] - [C])$	$2[A] - 2[C]$
$V_{xy} = V_{yx}$	0	0	0
$V_{xz} = V_{zx}$	$\frac{\sqrt{2}}{3}(-2[B] + [C])$	$\frac{\sqrt{2}}{3}(-2[A] + 2[C])$	0
$V_{yz} = V_{zy}$	0	0	0

be calculated using the partial quadrupole splitting equations given in Table I (*14*). Assuming pqs(A) = 0, pqs(B) can be calculated using the quadrupole splitting found for $Cr_{1.90}Al_{0.1}O_4$. For this sample, the only two tetrahedral configurations that are very probable are A_4 and AB_3. Thus the doublet (Fig. 2) with a QS of 0.74 mm/sec is due to the AB_3 configuration. We arbitrarily take pqs(A) = 0.0 and then use the AB_3 quadrupole splitting to solve for pqs(B) = ±0.37 mm/sec. The choice of reference value (pqs(A) = 0) and the sign of the QS values makes no difference to the calculated QS for other configurations. The pqs(B) is found to equal −0.37 assuming the quadrupole splitting is positive. If pqs(A) = 0 and pqs(B) is rounded to equal −0.40 for simplicity then pqs(C) is taken as −0.80 and pqs(D) as −1.20 (double and triple pqs(B) as in other iron-bearing compounds, see Ref. (*14*)). The rounding of the values chosen for pqs(B), pqs(C), and pqs(D) results in a small error in the calculated pqs values. However, this is considered small in comparison to errors associated with the simpli-

TABLE II

CALCULATED QUADRUPOLE SPLITTINGS AND CATION CONFIGURATION PROBABILITIES

Cation configuration	QS (mm/sec)	Probability of occurrence						
		Cr2.00	Cr1.90	Cr1.75	Cr1.50	Cr1.00	Cr0.50	Al2.00
$A_4 = B_4 = C_4 = D_4$	0.00	1.000	0.5807	0.2083	0.0638	0.0400	0.0638	1.000
$AB_3 = BA_3 = BC_3 = CB_3 = CD_3 = DC_3$	0.80	0.000	0.3202	0.4127	0.2976	0.2168	0.2976	0.000
$A_2B_2 = B_2C_2 = C_2D_2$	0.92	0.000	0.0738	0.2227	0.2115	0.1359	0.2115	0.000
$AC_3 = CA_3 = BD_3 = DB_3$	1.60	0.000	0.0176	0.0495	0.0484	0.0586	0.0484	0.000
$A_2C_2 = B_2D_2$	1.84	0.000	0.0002	0.0045	0.0215	0.0172	0.0215	0.000
$ABC_2 = A_2BC = BCD_2 = B_2CD$	1.41	0.000	0.0077	0.0673	0.1747	0.2110	0.1747	0.000
$AB_2C = BC_2D$	1.29	0.000	0.0012	0.0272	0.1288	0.1582	0.1288	0.000
$A_3D = AD_3$	2.40	0.000	0.000	0.000	0.0048	0.0020	0.0048	0.000
A_2D_2	2.76	0.000	0.000	0.000	0.0003	0.0015	0.0003	0.000
$A_2BD = ABD_2$	2.22	0.000	0.000	0.000	0.0149	0.0176	0.0149	0.000
$A_2CD = ACD_2$	2.77	0.000	0.000	0.000	0.0050	0.0176	0.0050	0.000
AB_2D	2.11	0.000	0.000	0.000	0.0144	0.0264	0.0144	0.000
AC_2D	2.55	0.000	0.000	0.000	0.0016	0.0791	0.0016	0.000

TABLE III

QUADRUPOLE SPLITTING EQUATIONS FOR $FeCr_2O_4$–$FeAl_2O_4$

$$QS_{Cr2.00} = 1.000(0) + 0.000(S) + 0.000(M) + 0.000(L)$$
$$QS_{Cr1.90} = 0.581(0) + 0.394(S) + 0.027(M) + 0.000(L)$$
$$QS_{Cr1.75} = 0.208(0) + 0.635(S) + 0.149(M) + 0.000(L)$$
$$QS_{Cr1.50} = 0.064(0) + 0.509(S) + 0.373(M) + 0.041(L)$$
$$QS_{Cr1.00} = 0.040(0) + 0.353(S) + 0.445(M) + 0.144(L)$$
$$QS_{Cr0.50} = 0.064(0) + 0.509(S) + 0.373(M) + 0.041(L)$$
$$QS_{Al2.00} = 1.000(0) + 0.000(S) + 0.000(M) + 0.000(L)$$

$S = 0.86$ mm/sec, $M = 1.54$ mm/sec, $L = 2.47$ mm/sec

fied Ingall's theory (Eq. (1)) and errors resulting from the actual fitting of the spectra. Quadrupole splittings for the 35 possible next-nearest neighbor configurations for *T*-site Fe^{2+} are then calculated using the equations given in Table II (see Appendix 1).

These quadrupole slittings can be organized into four groups, with $QS = 0$, 0.86, 1.54, and 2.47 mm/sec corresponding to zero, small, medium, and large quadrupole splitting, respectively. Assuming a random distribution of Al onto the octahedral sites and random distributions of *A*, *B*, *C*, and *D* orientations, the probabilities for occurrence of the next-nearest neighbor octahedral cation configurations, can be calculated and are listed in Table III with the resulting quadrupole splitting equations. It should be noted that some of the cation configurations such as ABD_2 which result in a more distorted EFG are no longer within the linear region of Eq. (1) (Fig. 5). In these cases, the calculated quadrupole splittings were plotted and extrapolated back to the curve calculated from Eq. (1) to arrive at the values reported here.

The calculated quadrupole splittings compare well with those obtained for unconstrained two peak fits (Tables III and IV). In the case of the calculated fits, areas of the peaks corresponding to each of the four groups of octahedral cation configurations were constrained to be proportional to the probability of their occurrence. Quadrupole splittings were also constrained to equal those calculated above. Figure 3 shows the fitted spectrum for sample Fe $CrAlO_4$. Quadrupole splittings and areas are constrained to equal those predicted by the calculation presented above. As can be seen, the absorption envelope derived for the sample is a good approximation to the data. The small deviations of the predicted spectral envelope from that experimentally observed can most likely be attributed to the Lorentzian lineshape of the fitted peaks. The actual lineshape of the absorption should most likely be Gaussian due to slight differences in *QS* between various configurations within each classification (small, medium, large).

The temperature dependence of each quadrupole splitting can also be calculated using the Eq. (1) and by inputting a different $QS(0)$ and Δ for each cation configuration. Δ for those cation configurations with values lying outside the linear region of Fig. 5 were extrapolated back to the curve. Others were deduced directly from the quadrupole splittings. The temperature dependence of each cation configuration is plotted in Fig. 6, as is the temperature dependence of the small, medium, and large averaged quadrupole splitting values. The

TABLE IV

OBSERVED AND CALCULATED SPECTRAL PARAMETERS

Sample	*IS*	*QS*	Γ_H	QS^a	QS^b
Cr2.00	0.90	0.00	0.33	0.00	0.00
Cr1.90	0.91	0.00	0.42	—	—
Cr1.75	0.92	0.79	0.65	0.79	0.78
Cr1.50	0.94	0.91	0.79	0.91	1.11
Cr1.00	0.90	1.85	0.30	1.28	1.35
	0.94	1.34	0.54		
	0.96	0.75	0.54		
	0.94	0.91	0.79		
Cr0.50				0.91	1.11

Note. *IS*, *QS*, Γ_H (in mm/sec), *IS* relative to iron foil.

[a] Two-peak fit.

[b] Calculated fit from equations of Table III.

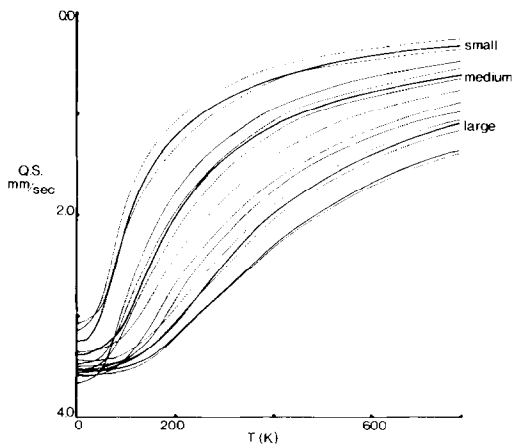

FIG. 6. Temperature dependence of individual and average T site quadrupole splitting (QS), calculated from Eq. (1).

quadrupole splittings of the various cation configurations is predicted to decrease with temperature as observed (Fig. 4). Application of the additive model already outlined to high and low temperature spectra produces good agreement between observed quadrupole splittings for unconstrained two peak fits and those predicted by the present theory (Fig. 7).

The resolution of an inner doublet with narrower half-width and lower quadrupole splitting in the 110 K spectrum of $FeCrAlO_4$ could be predicted from Fig. 4. This shows a clear separation at low temperature of the A_2B_2 and AB_3 octahedral cation arrangements (those grouped as QS = 0.86 for room temperature small QS). The other cation arrangements with high probability of occurrence (AB_2C, AC_3, ABC_2, and AC_2D) form more of a continuous spectrum of values with medium/large predicted QS. At higher temperatures resolution of individual doublets would be predicted to decrease as we actually observe.

Discussion

The question of whether the third (and greater) coordination sphere cations induce an electric field anisotropy about the T-site Fe^{2+} nucleus must be addressed. Partial quadrupole splitting (pqs) calculations have been previously based solely on the premise that differences in electronic structure of the substituent atom result in a change in effective charge distribution about the Mössbauer atom. Thus, long-range effects would not be expected. However, we recognize that differences in atomic radii of substituent and substituted atoms must result in some degree of bond strain. This can be theoretically quantified in terms of atomic displacements about the atomic species introduced. Dollase (*15*) concluded from theoretical argument that the most significant displacement is that of atoms directly bonded to the substituent atom. Atomic displacement falls off rapidly with increasing distance from the substituted site (displacement is approximately inversely proportional to the square of the interatomic distance). If atomic displacement at one bond length is taken as 100%, at two it is 10%, and at four less than 1%. The difference in atomic radius of a substituent atom (e) causes the atoms bonded to it to move toward or away by some fraction of e. The degree of accommodation of substituent is termed the "site compliance" by

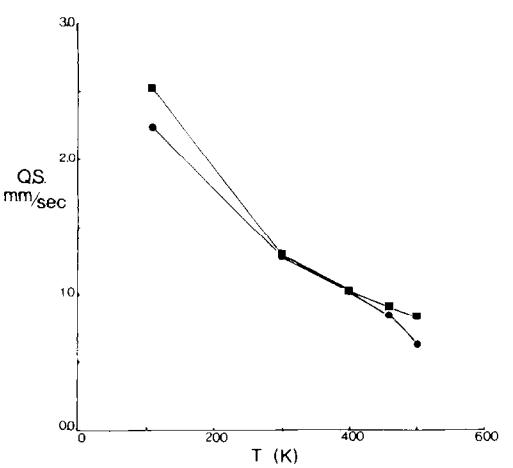

FIG. 7. Observed (circles) and calculated (squares) quadrupole splitting (QS) for $FeCrAlO_4$ at various temperatures (see Fig. 4).

Dollase and was found by him to be approximately 50% for the rock salt structure. Dollase also found that the more highly connected the structure, either by increased coordination number or by increased numbers of shared polyhedral edges or faces, the lower the compliance around a replaced atom. The site compliance correlates best with the coordination number of the ligands surrounding the replaced atom itself. On this basis, compliance for spinels can be estimated at approximately 70% for the oxygen atoms bonded to a substituent *M*-site cation and 7% at the third coordination sphere tetrahedral cation site. The numbers presented here do seem to rule out the effects of the next-next-nearest neighbor sphere on the Mössbauer spectra of the (Cr,Al) spinels. This supports the conclusions already deduced from the lack of quadrupole splitting induced by tetrahedral substitution in the $(Fe,Mg)Cr_2O_4$ and $(Fe,Zn)Cr_2O_4$ systems (*16*). However, long-range distortion could possibly reduce the number of *T*-site cations experiencing a zero or small EFG which would result in diminution of singlet peak area in the Fe $Cr_{1.75}Al_{.25}O_4$ sample (Fig. 1). A singlet with probable area of 0.21 is predicted from next-nearest neighbor calculations to be present in the spectrum of this sample, but is not resolved. It should be noted however that a singlet of approximately the predicted area is found in the $FeCr_{1.75}Rh_{0.25}O_4$ spectrum reported by Reidel and Karl (*9*).

Substituent atom accommodation can also be used to qualitatively discuss the size of induced quadrupole splitting by next-nearest neighbor substitution and the degree of resolution of component next-nearest neighbor doublets in various spinel systems. Table V contains ionic radii and electronegativities for a number of *M*-site cations in spinels whose Mössbauer spectra have been reported. For normal spinels, *T*-site quadrupole splittings of (Cr, Al) spinels are larger than those of (Cr, Fe^{3+}) spinels. This can be related to the difference in substituent cation radii. The ionic size difference between Cr^{3+} and Al is −0.23 Å and between Cr^{3+} and Fe^{3+} it is +0.03 Å. This results in bond length changes of +0.016 and −0.002 Å, respectively, at the *T*-site. The differences in quadrupole splittings and component doublet resolution between the (Cr, Al) spinels and the (Cr, Rh) thiospinels could be attributed to difference in cation radii but they are better explained by the greater degree of polarizability of the sulfide anion.

TABLE V

CATION RADII AND ELECTRONEGATIVITIES FOR SOME SELECTED ATOMIC SPECIES

Cation	Radius[a] (Å)	Electronegativity[b]
Al^{3+}	0.39	1.61
Cr^{3+}	0.615	1.66
Fe^{3+}	0.645	1.83
Rh^{3+}	0.665	2.28
Se^{2-}	1.98	2.55
S^{2-}	1.84	2.58
O^{2-}	1.40	3.44

[a] Refs. (*18, 19*).
[b] Ref. (*20*).

Another interesting comparison can be made between the Mössbauer spectra of $Fe(Cr,Rh)_2S_4$ thiospinels and of $FeCr_2(S_{1-x}Se_x)_4$ composition spinels (with $x = 0$ to 0.3) (*17*). In $Fe(Cr,Rh)_2S_4$, a large quadrupole splitting is induced by the substitution of Rh^{3+} for Cr^{3+} (electronegativities 2.28 and 1.66, respectively). In $FeCr_2(S_{1-x}Se_x)_4$, three sets of doublets are induced by the introduction of Se for S and are assigned to ligand configurations of S_4, S_3Se, and S_2Se_2. All three configurations produce doublets of smaller quadrupole splitting than those produced by Rh^{3+} substitution into the next-nearest neighbor cation sphere. In agreement with the Mössbauer spectra, the difference in electronegativity between S and Se (0.03) is much less than the difference in electronegativity between Cr^{3+} and Rh^{3+}. On the

other hand, the difference in ionic radii of S^{2-} and Se^{2-} (+0.14 Å) is greater than that of Cr^{3+} and Rh^{3+} (+0.05). Also, since the anions are in the first coordination sphere, a much larger site compliance would be expected for the S/Se substitution. Thus, bond character appears to have a more significant effect than substituent atom accommodation on the EFG of *T*-site Fe^{2+} cations in chalcogenide spinels.

Conclusions

Systematic Fe^{2+} *T*-site quadrupole splittings in the Mössbauer spectra of synthetic chromite-hercynite spinels ($Fe(Cr_{1-x}Al_x)_2O_4$, with $x = 0$ to 1.5) are reported and analyzed.

A narrow singlet in $FeCr_2O$ develops into a singlet with broad shoulders with $x = 0.10$, and into a broad resolved asymmetric doublet with $x = 0.25$. Maximum quadrupole splitting and peak half-width are associated with $x = 1.0$.

These effects are attributed to substitution of octahedrally coordinated (*M* site) cations in the next-nearest neighbor coordination sphere causing *local* charge distortion about *T*-site cations. Mössbauer spectra with $x \neq 0.0$ are therefore composite. Assuming random distribution of octahedral cations, the probabilities for occurrence of the 35 possible next-nearest neighbor configurations have been calculated for given bulk compositions. For the first time, we have used partial quadrupole splitting (pqs) theory to calculate the quadrupole splittings for the different configurations. Application of the pqs theory is facilitated by the restricted number of quantitatively significant configurations in bulk compositions with low x, e.g., for $FeCr_{1.90}Al_{0.10}O_4$, only A_4 and AB_3 configurations (where *A* is 3Cr and *B* is 2CrlAl) are quantitatively important. Further simplification is afforded by organizing the quadrupole splittings of the 35 possible site distortions into just four groups of zero, small, medium, and large quadrupole splittings.

Calculated bulk quadrupole splittings are in good agreement with those obtained for unconstrained two peak fits, at room temperature and at low and high temperatures. Also, predicted spectral details, concealed within broadened peaks at room temperature, are resolved in 110 K spectra.

In $Fe(Cr_{1-x}Al_x)_2O_4$ spinels, anisotropy of the electric field about *T*-site Fe^{2+} cations (and thus the quadrupole splitting) is clearly related to distortion associated with spatial accommodation of substituent Al^{3+} cations. However, in (Cr, Rh) chalcogenide spinels, difference in bond character may have a more significant effect.

Appendix 1: Sample Calculation of Quadrupole Splitting from Partial Quadrupole Splittings

We will use the ABC_2 next-nearest neighbor configuration with pqs(*A*) = 0.0, pqs(*B*) = −0.40, and pqs(*C*) = −0.80 mm/sec as an example. The pqs values are related to the components of the electric field gradient tensor (*E*), V_{xx}, V_{yy}, V_{zz}, and V_{xz}, using the equations in Table I (given in quadrupole splitting units).

$$\mathbf{E} = \begin{bmatrix} -0.1233 & 0 & -0.3488 \\ 0 & -1.11 & 0 \\ -0.3488 & 0 & 1.2333 \end{bmatrix} \quad (2)$$

This matrix is diagonalized by solving the quadratic equation for **E** and a new matrix constructed taking $|V_{xx}|$ as the smallest value obtained for **E** and $|V_{zz}|$ as the largest value obtained

$$\mathbf{E} = \begin{bmatrix} -0.2077 & 0 & 0 \\ 0 & -1.11 & 0 \\ 0 & 0 & 1.3177 \end{bmatrix} \quad (3)$$

"η," the asymmetry parameter, is calculated from the relationship

$$\eta = \frac{V_{xx} - V_{yy}}{V_{zz}} = 0.6848 \qquad (4)$$

Finally, the quadrupole splitting for the ABC_2 next-nearest neighbor configuration is given by

$$QS = 1.3177\left(1 + \frac{0.6848^2}{3}\right)^{1/2} = 1.4169 \text{ mm/sec} \qquad (5)$$

References

1. K. Ono, A. Ito, and Y. Syono, *Phys. Lett.* **19,** 620 (1966).
2. K. Ono, L. Chandler, and A. Ito, *Phys. Lett. A* **24,** 273 (1967).
3. D. S. McClure, *J. Phys. Chem. Solids* **3,** 311 (1957).
4. F. Hartmann-Boutron and P. Imbert, *J. Appl. Phys.* **39,** 775 (1968).
5. J. B. Goodenough, *J. Phys. Chem. Solids* **25,** 151 (1964).
6. G. M. Bancroft, M. D. Osborne, and M. E. Fleet, *Solid State Commun.*, **47,** 623 (1983).
7. T. Mizoguchi and M. Tanaka, *J. Phys. Soc. Jpn.* **18,** 1301 (1963).
8. M. Robbins, G. K. Wertheim, R. C. Sherwood, and D. W. E. Buchanan, *J. Phys. Chem. Solids* **32,** 717 (1971).
9. E. Riedel and R. Karl, *J. Solid State Chem.* **35,** 77 (1980).
10. G. M. Bancroft and R. H. Platt, *Advan. Inorg. Radiochem.* **15,** 59 (1972).
11. M. D. Osborne, M. E. Fleet, and G. M. Bancroft, *Contrib. Mineral. Petrol.* **77,** 251 (1981).
12. R. Ingalls, *Phys. Rev. A* **133,** 787 (1964).
13. T. C. Gibb and N. N. Greenwood, *J. Chem. Soc.* 6989 (1965).
14. G. M. Bancroft, K. D. Butler, and A. T. Rake, *J. Organomet. Chem.* **34,** 137 (1972).
15. W. A. Dollase, *Phys. Chem. Miner.* **6,** 295 (1980).
16. M. D. Osborne, M. E. Fleet, and G. M. Bancroft, *Solid State Commun.*, **48,** 663 (1983).
17. E. Riedel, A. Al-Juani, R. Rackwitz, and H. Suchtig, *Z. Anorg. Allg. Chem.* **480,** 49 (1981).
18. R. D. Shannon, *Acta Crystallogr. Sect. A* **32,** 751 (1976).
19. L. Pauling, "The Nature of the Chemical Bond," ed. 3, Cornell Univ. Press, Ithaca, N.Y.
20. A. L. Allred, *J. Inorg. Nucl. Chem.* **17,** 215 (1961).